

Changes in water age during dry-down of a non-perennial stream

Co-author list: Logan J. Swenson^{1,2,*}, Sam Zipper^{1,*}, Delaney M. Peterson³, C. Nathan Jones³, Amy J. Burgin⁴, Erin Seybold¹, Matthew F. Kirk⁵, Camden Hatley^{1,2}

Affiliations:

1. Kansas Geological Survey, University of Kansas
2. Department of Geology, University of Kansas
3. Department of Biological Sciences, University of Alabama
4. Kansas Biological Survey-Center for Ecological Research, University of Kansas
5. Department of Geology, Kansas State University

* Corresponding authors: loganswenson@ku.edu, samzipper@ku.edu

Author ORCID IDs:

Swenson: 0000-0003-4981-3478

Zipper: 0000-0002-8735-5757

Peterson: 0000-0002-3444-4772

Jones: 0000-0002-5804-0510

Burgin: 0000-0001-8489-4002

Seybold: 0000-0002-0365-2333

Kirk: 000-0001-5562-7618

Hatley: 0000-0001-9840-2734

This is a non-peer-reviewed manuscript being submitted to Water Resources Research.

Key points:

- Stream isotopic composition was progressively enriched in $\delta^{18}\text{O}$ and $\delta^2\text{H}$ as the stream network dried.
- Stream isotopic enrichment is caused by evaporative effects and a decrease in surface water connectivity.
- Most streamflow was young water (stored in the subsurface < 3 months), with older and more variable water age as the stream network dried.

33 **Abstract:**

34 Non-perennial streams, which lack year-round flow, constitute more than half the global stream
35 network length. Identifying the sources of water that sustain flow in non-perennial streams is necessary
36 to understand their potential impacts on downstream water resources, information that is needed to
37 guide water policy and management. Here, we used water isotopes ($\delta^{18}\text{O}$ and $\delta^2\text{H}$) to partition the
38 evolution of streamwater age compositions and inferred sources through the 2021 summer dry-down
39 period of a non-perennial stream network at Konza Prairie (KS, USA). During dry-down, the isotopic
40 composition of non-perennial streams was progressively enriched in $\delta^{18}\text{O}$ and $\delta^2\text{H}$. Using a Bayesian
41 unmixing approach,, we found a substantial amount of summer streamflow (mean 55.2%) is young
42 water that had been stored in the subsurface for less than ~ 3 months. Streamwater shifted to older
43 sources and variability in age increased as summer progressed, with young water ranging from 53.9% to
44 62.6% (June) and 39.1% to 62.0% (August). The shift in water age suggests a shift away from rapid
45 fracture flow towards slower matrix flow that creates a sustained but localized surface water presence
46 during late summer and is reflected in the annual dynamics of water age at the catchment outlet. The
47 substantial proportion of young water highlights the vulnerability of non-perennial streams to short-
48 term hydroclimatic change, while the late-summer shift to older water reveals a sensitivity to longer-
49 term changes in groundwater dynamics. Combined, this suggests that local changes may propagate
50 through non-perennial stream networks to influence downstream water availability and quality.

51 **Plain Language Summary:**

52 Non-perennial streams, which periodically cease to flow, are widespread globally. Identifying the origin
53 and age of water in non-perennial streams will help guide water policy and management strategies. We
54 used water isotopes ($\delta^{18}\text{O}$ and $\delta^2\text{H}$), a common hydrologic tracer, to identify stream water sources and
55 age during the 2021 summer dry-down period of a non-perennial watershed at the Konza Prairie (KS,
56 USA). We found that water sources and flowpaths changed as the stream network dried. Approximately
57 half of summer streamflow is young water, meaning it took less than 3 months to travel from
58 precipitation to the stream. However, as the summer progressed, streamwater shifted to older sources.
59 We interpret this shift in the water age to indicate a shift in the source of water from rapid flowpaths
60 early in the summer, to slower flowpaths later in the summer, which sustain localized surface water
61 during the driest parts of the year. Taken together, the substantial amount of young water highlights the
62 vulnerability of non-perennial streams to short-term weather changes and longer-term changes in
63 groundwater dynamics that can alter the quantity and quality of water flow through non-perennial
64 stream networks to ultimately influence downstream water availability and quality.

65 1. Introduction

66 Non-perennial streams, including intermittent and ephemeral streams, which do not flow year-
67 round (Busch et al., 2020), constitute more than half the global stream network length (Messenger et al.,
68 2021), and are becoming more common worldwide due to water abstraction and climate change (Zipper
69 et al., 2021; Trambly et al., 2021). Given their global prevalence and their shifts between aquatic
70 (flowing) and terrestrial (dry) conditions, non-perennial streams can strongly influence the ecological
71 health of river networks through regulation of biogeochemical cycles of nutrients and organic matter
72 (Hale and Godsey, 2019; Zimmer and McGlynn, 2018) and local and downstream water quality and
73 quantity (Gómez et al., 2017; Zimmer et al., 2022). Despite their importance, non-perennial streams are
74 overlooked, undermonitored, and understudied (Krabbenhoft et al., 2022). However, growing
75 recognition of their abundance has driven attempts to refine hydrological and ecological theories to
76 account for the unique characteristics of non-perennial flow regimes (Shanafield et al., 2021; Allen et al.,
77 2020), particularly related to the patterns and dynamics of stream drying (Price et al., 2021).

78 While a growing number of contemporary studies have highlighted the important and unique
79 role of non-perennial streams on watershed hydrologic and ecological function, management of and
80 policy affecting these systems remains contested and unclear (Walsh and Ward, 2022). In the US, federal
81 policy debates over non-perennial stream protections focus on “significant connectivity” between non-
82 perennial streams and downstream 'navigable' waters (Alexander, 2015). Since 2015, three different
83 Environmental Protection Agency rules have been used to define protections of non-perennial streams -
84 - resulting in repeated disagreement and reversal of protections (Ward et al. 2023). Definitions of
85 protected waters have considered if they have a “significant nexus” (Clean Water Rule, 2015), if they are
86 "relatively permanent" (Navigable Waters Protection Rule, 2020), or more recently with new US federal
87 protections that allowed either the “relatively permanent standard” or “significant nexus standard” to
88 classify protected waters (Revised Definition of “Waters of the United States”, 2023). However, the
89 newly revised federal policy that expanded protections for non-perennial streams has already been
90 overturned in the Supreme Court, leading to an uncertain future for non-perennial stream protection
91 and management in the US (Liptak, 2023). Globally, this policy debate is mirrored in other regions. For
92 example, in the European Union, the inclusion and protection of non-perennial streams in management
93 frameworks is still emerging and varies widely between member countries (Leone et al., 2023). These
94 policy debates highlight the need to better characterize the hydrology of non-perennial streams and
95 quantify their impact on both local and downstream ecosystem function.

96 Quantifying the connection between non-perennial streamflow and water quality first requires
97 an understanding of the origin of water in these streams and the timescales over which water is
98 transmitted to the stream (Hrachowitz et al., 2016), which affects, for example, redox processes
99 (Zarnetske et al., 2011) and mineral weathering rates (Maher, 2010). While water age methods exist at
100 temporal scales that are suitable for non-perennial streams, such as event-based hydrograph separation
101 (Klaus and McDonnell, 2013), they only give information about water age during storm events. Many
102 other age methods, such as the young water fraction (Kirchner, 2016) and time-variable StorAge
103 Selection (SAS) functions (Harman, 2015), require sampling at a high-temporal frequency (e.g., weekly)
104 to fit timeseries-based models or probability distributions that are potentially not suitable for non-
105 perennial streams (Xia et al., 2023; Benettin et al., 2022), which often flow seasonally or in response to
106 precipitation events and therefore can have long periods where samples cannot be collected (Shanafield
107 et al., 2021; Costigan et al., 2016). Furthermore, many previous water age and source estimates often
108 integrate age and source to a single measurement point at the watershed outlet, thereby failing to
109 capture the potential variation in the spatial distribution of water within a network (Jensen et al., 2019;
110 Botter and Durighetto, 2020). Thus, quantifying the within-network spatial and temporal evolution of
111 water age and sources in non-perennial streams underpins our ability to predict the vulnerability of
112 these systems to changes in groundwater dynamics and streamflow which are exacerbated by changing
113 climate and human activities (Zipper et al., 2022; Datry et al., 2022). Ultimately, understanding the age
114 and source of water in non-perennial streams can help determine when and how they will impact water
115 quantity and quality in downstream waters. For example, understanding the source of late summer
116 baseflow could direct nonpoint source pollution management activities to improve water quality.

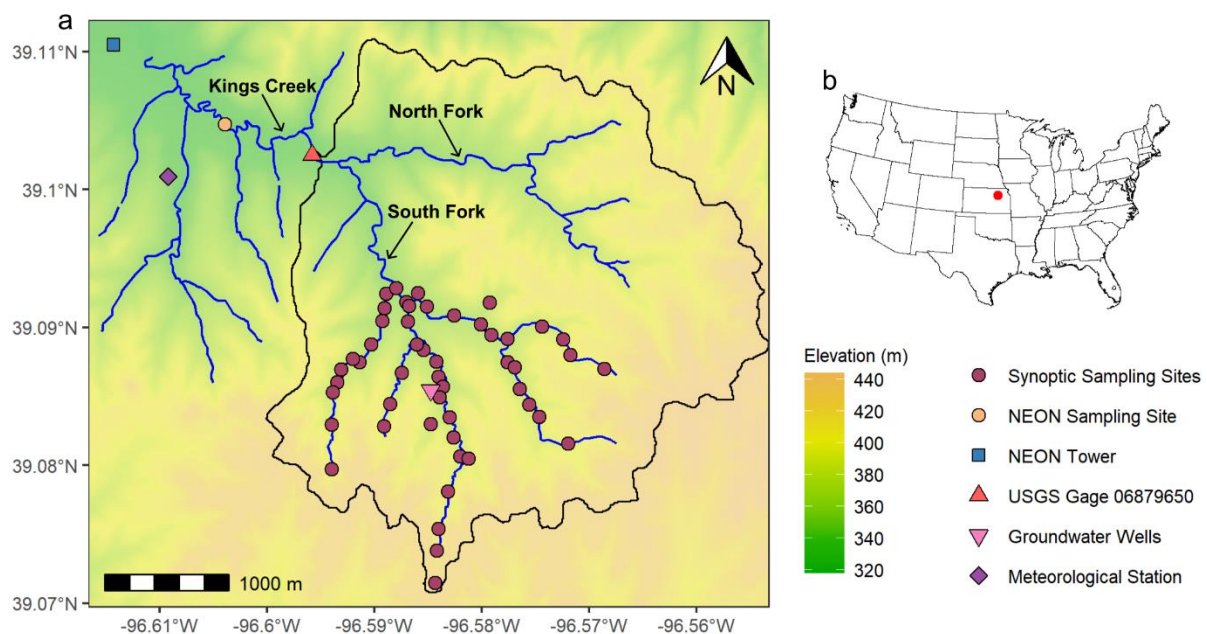
117 To advance this this understanding, our goal was to quantify the spatiotemporal variability in
118 stream isotopic composition and water age, and infer changes in water source, during the dry-down of a
119 non-perennial stream network at the Konza Prairie Biological Station (Kansas, USA). Specifically, we
120 asked three questions: (1) How do streamwater isotopic compositions in non-perennial streams vary
121 spatially and temporally? (2) What factors most strongly influence the distribution of isotopic
122 compositions in non-perennial streams, and how do these factors vary through time? (3) What does this
123 imply about the sources of water and their transit times sustaining streamflow? We answered these
124 questions using water isotopes ($\delta^{18}\text{O}$ and $\delta^2\text{H}$), a commonly applied hydrologic tracer for identifying
125 water sources and modeling water age (Jasechko, 2019), in a Bayesian unmixing model to infer water
126 age over both time and space. We applied this model to isotopic samples that were collected through

127 regular sampling at the watershed outlet and three spatially-dense synoptic campaigns throughout
128 summer 2021 to evaluate both spatial and temporal dynamics in water age as the stream network dried.
129

130 2. Data and Methods

131 2.1. Study Site

132 This study analyzes the 2021 summer dry-down of Kings Creek at the Konza Prairie Biological
133 Station in the Flint Hills ecoregion of Kansas, USA (Figure 1). Konza Prairie is a native tallgrass prairie,
134 part of the National Ecological Observatory Network (NEON) and is a Long Term Ecological Research
135 (LTER) site. The terrain is merokarst with thin limestone units (1-2 m thick) interbedded with
136 mudstone/shale units (2-4 m thick), and is characterized by flashy stream responses to precipitation
137 events, preferential flow through conduits, and strong vertical heterogeneity (Sullivan et al., 2020; Vero
138 et al., 2018; Macpherson 1996). The landscape is terraced with more resistant limestone units forming
139 benches on hillslopes and knickpoints in stream channels, while less resistant mudstones erode to more
140 gradual slopes (Costigan et al., 2015). Soils are predominantly silty-clay loams; however, bedrock
141 commonly outcrops at the surface (Ransom et al., 1998). Soil profiles are deepest at the base of slopes
142 (~2 m) and are thinnest on the ridges (<20-50 cm) (Ransom et al., 1998).

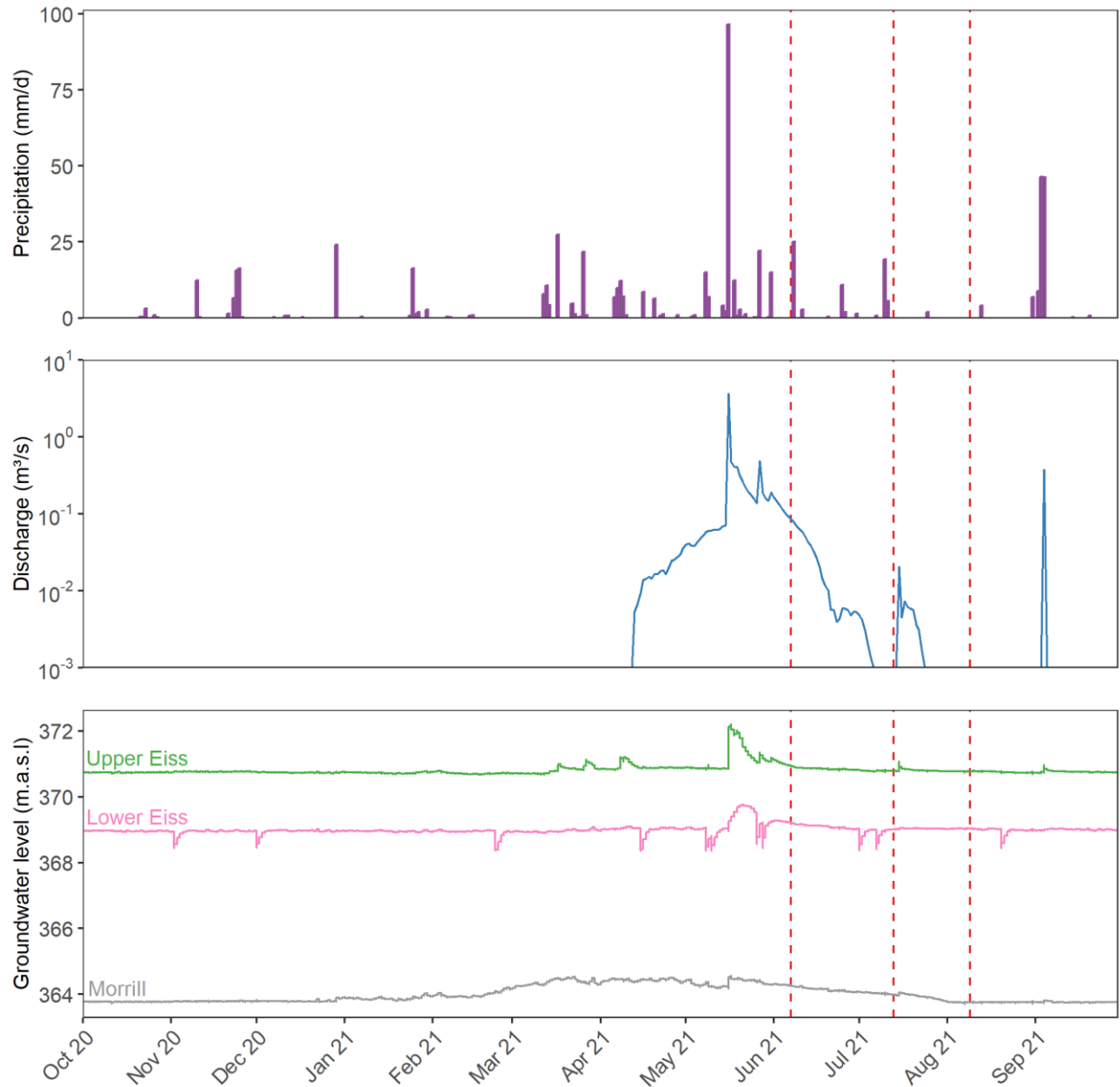


143
144 **Figure 1.** (a) Sampling sites and infrastructure along Kings Creek in the Konza Prairie, KS, USA. Stream
145 isotopes were collected in the headwaters of the South Fork of Kings Creek (Synoptic Sampling Sites),
146 while long-term samples were taken further downstream in Kings Creek (NEON Sampling Site).

147 Precipitation isotopes were collected as composite samples from a wet deposition collector (NEON
148 Tower). The outlet of the North and South Forks of Kings Creek has been monitored by the U.S.
149 Geological Survey since 1979 (USGS Gage 06879650) with a drainage area of 1150 ha of tall grass prairie.
150 Note: The groundwater well nest is offset 50 m away from the stream to be visible. (b) Location of the
151 Konza Prairie in the US.

152

153 The climate is mid-continental with cold, dry winters and warm, humid summers (Vero et al.,
154 2018). Average annual precipitation is 835 mm, with ~75% of rainfall occurring between April and
155 September, when vegetation is active and evapotranspiration rates are high (Hayden, 1998). Water lost
156 to evapotranspiration is the primary fate of water, representing ~70% of rainfall (~600 mm as
157 determined by eddy covariance measurements under long-term conditions; Logan and Brunsell, 2015).
158 Konza Prairie received 632 mm precipitation in the 2021 calendar year (76% of the annual average,
159 Figure 2); however, it was unequally distributed throughout the year. Spring (March-April) was very wet
160 (85 percentile of 30 year conditions) while the summer was very dry (2.5 percentile of 30 year
161 conditions). 1150 ha of tall grass prairie is drained by Kings Creek, a fifth order stream which has been
162 monitored by the U.S. Geological Survey (USGS) since 1979 (USGS gage 06879650). The Kings Creek
163 network dries in many, but not all, years between approximately July and September due to a decrease
164 in precipitation and increase in evapotranspiration (Costigan et al., 2015). Groundwater wells are
165 screened in the Upper and Lower Eiss and Morrill limestone units (stratigraphic unit names), which past
166 work found to contribute considerable amounts of groundwater to the stream at mid-elevations in the
167 South Fork of Kings Creek via springs along the hillslopes and within the streambed (Hatley et al., 2022).
168 Due to the karstic nature of these limestone units and well-developed but localized stream-aquifer
169 connections, discharge and groundwater levels respond quickly to precipitation events, with the initial
170 response typically occurring within 2 h of the event and peaking between 2.5 and 5 h afterwards (Hatley
171 et al., 2022; Brookfield et al., 2016). Based on pressure responses and rising-head slug tests in the
172 groundwater wells, the Upper Eiss Limestone appears to have slightly higher hydraulic conductivity than
173 the Morrill Limestone (10^{-5} to 10^{-4} m d⁻¹ for the Upper Eiss compared to 10^{-5} to 10^{-3} m d⁻¹ for the Morrill),
174 with both having greater hydraulic conductivity and stream connectivity than the Lower Eiss Limestone
175 (10^{-8} to 10^{-5} m d⁻¹ for the Lower Eiss) (Figure 2; Barry, 2018; Pomes, 1995).



176
 177 **Figure 2.** Timeseries of (a) precipitation, (b) discharge at USGS gage 06879650, and (c) groundwater
 178 levels at the Konza Prairie. Sampling events are shown as vertical dashed lines. Sharp declines in
 179 groundwater levels in the Lower Eiss occurred as a result of periodic sampling events and slow recovery
 180 in this low-conductivity unit.

181
 182 **2.2. Sampling Design & Ancillary Data**
 183 Water isotopes ($\delta^{18}\text{O}$ and $\delta^2\text{H}$) were collected on June 7th, July 13th, and August 9th (2021) as part
 184 of three day-long, spatially-distributed synoptic campaigns designed to capture a range of surface water

185 connectivity conditions during the dry-down of a non-perennial stream network. We identified 50
186 sampling sites spanning a range of drainage area and topographic wetness index, which have been
187 previously shown to be significant predictors of flow permanence in non-perennial streams (Warix et al.,
188 2021). A subset of the locations strategically targeted sites with long-term data, known springs, and
189 other locations of interest (see supplemental section S1 for full details on the sampling design). The
190 synoptic samples were collected only on the South Fork of Kings Creek, and the most downstream
191 synoptic network sampling point represented a drainage of 531 ha. On each sampling date, we visited all
192 50 sampling sites and collected samples if water was present, along with ancillary information regarding
193 the hydrologic conditions (i.e., whether the water was flowing or pooled and water temperature). A
194 total of 77 distinct grab samples, excluding replicates, were obtained: 43 samples in June, 19 samples in
195 July, and 15 samples in August. All samples were stored in 60-mL glass vials with conical inserts and
196 capped without headspace to prevent isotopic fractionation. Samples were kept in dark and at room
197 temperature (<20 °C) until analysis.

198 Additional data were compiled from the USGS, National Ecological Observatory Network
199 (NEON), and the Konza Prairie Long Term Ecological Research (LTER) programs. Discharge in Kings Creek
200 was obtained from USGS gage 06879650, which is ~1.6 km downstream from the most downstream
201 point of our synoptic sampling (Figure 1). Composite precipitation isotopes were collected
202 approximately every two weeks between November 2018 and September 2021 from a wet deposition
203 collector at the NEON Tower, with a gap in collection from March 2020 to July 2020 during the onset of
204 the COVID-19 pandemic (n = 45; Figure 1; NEON, 2022). The precipitation-sampling collectors meet
205 International Atomic Energy Agency (IAEA) recommendations to prevent evaporation. In addition to the
206 precipitation isotopes, stream isotopes were collected approximately every two weeks over the 2021
207 water year at the NEON Sampling Site (n = 22; Figure 1; NEON, 2022), which is ~1.1 km downstream of
208 the USGS gage, and has a contributing area of 1306 ha. The USGS and NEON measurement points had
209 substantially larger contributing areas, incorporating both the North and South Fork of Kings Creek,
210 while the synoptic samples were only in the South Fork. NEON precipitation and stream isotopes were
211 stored in dark, cool (<20 °C) conditions and analyzed at the SIRFER Lab at University of Utah. Daily
212 precipitation amounts were recorded at the Konza Prairie Headquarters meteorological station (Figure
213 1; Nippert, 2022). Groundwater levels were logged at 5-min intervals in the Upper Eiss, Lower Eiss, and
214 Morill limestone aquifers (Figure 1; Hatley et al., 2022). The meteorological and groundwater data
215 collection networks are maintained by the Konza Prairie LTER program.

216 2.3. Lab Analysis

217 Surface water isotopes were measured using a cavity ring-down spectroscopic isotopic water
218 analyzer (Picarro L2130-*i*, Picarro Inc., CA). In order to account for memory effects, each sample was run
219 as six sub-samples. The first three sub-samples were used to equilibrate the cavity (and therefore were
220 excluded from the analysis), whereas the last three sub-samples were averaged to calculate sample
221 isotopic compositions. To account for instrument drift and precision, all samples were calibrated against
222 internal secondary standards, which were run repeatedly every 6 samples. Internal secondary standards
223 were calibrated against the IAEA primary standards for Vienna Standard Mean Ocean Water (VSMOW;
224 $\delta^{18}\text{O} = 0.0\text{‰}$, $\delta^2\text{H} = 0.0\text{‰}$). Average instrument precision was calculated as 0.05‰ and 0.41‰ for $\delta^{18}\text{O}$
225 and $\delta^2\text{H}$ respectively based on the comparison of 41 total duplicate internal secondary standards.
226 Isotopes values were reported in parts per thousand (‰) deviation relative to VSMOW:

$$227 \delta = (R_s/R_{\text{std}} - 1) * 1000$$

228 where R_s and R_{std} are the isotope ratio ($^2\text{H}/^1\text{H}$ or $^{18}\text{O}/^{16}\text{O}$) in the samples and standard (VSMOW)
229 respectively (Craig, 1961).

230 Deuterium excess (d-excess) was calculated for each sample as $d\text{-excess} = \delta^2\text{H} - 8 \times \delta^{18}\text{O}$, where
231 d-excess values less than 10 (i.e., the intercept of the Global Meteoric Water Line) indicate a sample has
232 been partially evaporated (Dansgaard, 1964). We choose d-excess to detect evaporation because the
233 Local Meteoric Water Line at the Konza Prairie has a similar slope and intercept as the Global Meteoric
234 Water Line (LMWL: $\delta^2\text{H} = 7.93 \times \delta^{18}\text{O} + 10.28$, $R^2 = 0.97$; Figure S5).

235

236 2.4. Bayesian Unmixing

237 In this study, we conducted a point-based water age estimation using a Bayesian unmixing
238 approach to investigate both the spatial dynamics and average catchment outlet processes of water age.
239 Bayesian unmixing was applied to the synoptic samples in the headwaters of the South Fork of Kings
240 Creek to observe spatial dynamics of water age during stream drying, and to the long-term NEON
241 samples at the catchment outlet to observe temporal changes of water age. We used the mixing-
242 evaporation model outlined in Bowen et al. (2018) to estimate the proportion of streamwater less than
243 ~3 months in age at each sampling point during drying. In doing so, we assumed that the isotopic signal
244 in streamwater reflects an integrated mix of seasonally-distinct precipitation signals, dependent on their
245 pathways to streamflow. We defined two amount-weighted sources contributing to streamflow: (1)
246 precipitation that fell less than ~3 months ago and (2) precipitation older than 3 months. These age
247 distributions were chosen to split precipitation into two isotopically-distinct sources, where the

248 distribution for less than ~3 months in age represents the isotopic properties of spring/early summer
249 precipitation, while the distribution for greater than ~3 months in age represents the isotopic properties
250 of the long-term average precipitation. Groundwater was not included as a separate endmember in the
251 unmixing analysis. Due to the non-perennial nature of our study site and unequal distribution of
252 precipitation between spring and fall (Figure 2), this method is well-suited for our study site.

253 The mixing-evaporation model (*mixSource*) is available in the *isoWater* package in R (Bowen,
254 2022) and uses Markov Chain Monte Carlo sampling to generate a posterior distribution of source
255 mixtures conditioned on the observed isotopic values. In brief, the model predicts the measured isotopic
256 composition (δ_{obs}) of a water sample from the values of an unevaporated source water (δ_s) as:

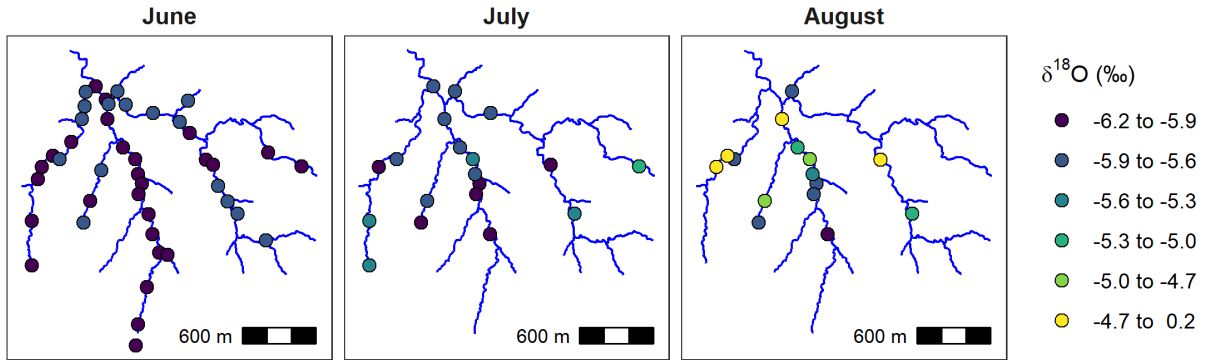
$$257 \quad \delta^{18}O_{obs} = \delta^{18}O_s + E$$

$$258 \quad \delta^2H_{obs} = \delta^2H_s + E \times m$$

259 where E is an evaporation index (in units of $\delta^{18}O$) and m is the slope of the evaporation line (EL). Prior
260 estimates are provided for each term on the right side of the equations, and the model is inverted using
261 Bayes Rule to obtain a posterior distribution for all model parameters conditioned on the observed
262 sample values. Prior estimates were provided to the package for the two precipitation sources
263 represented as bivariate normal distributions and the evaporation line represented by a normal
264 distribution. The slope of the evaporation line ($m = 6.00 \pm 0.55$) was estimated as a linear regression fit
265 to the stream isotopes during the summer dry-down ($R^2 = 0.99$; Figure S5). The prior describing the
266 relative contributions of each source was left uniformed. For all analyses, three chains were generated,
267 each run to a length of 200,000 samples with thinning to retain 7,500 samples per chain. Convergence
268 was assessed with the R-hat statistic ($R\text{-hat} < 1.05$) and effective sample size (mean = 930), indicating
269 good model convergence.

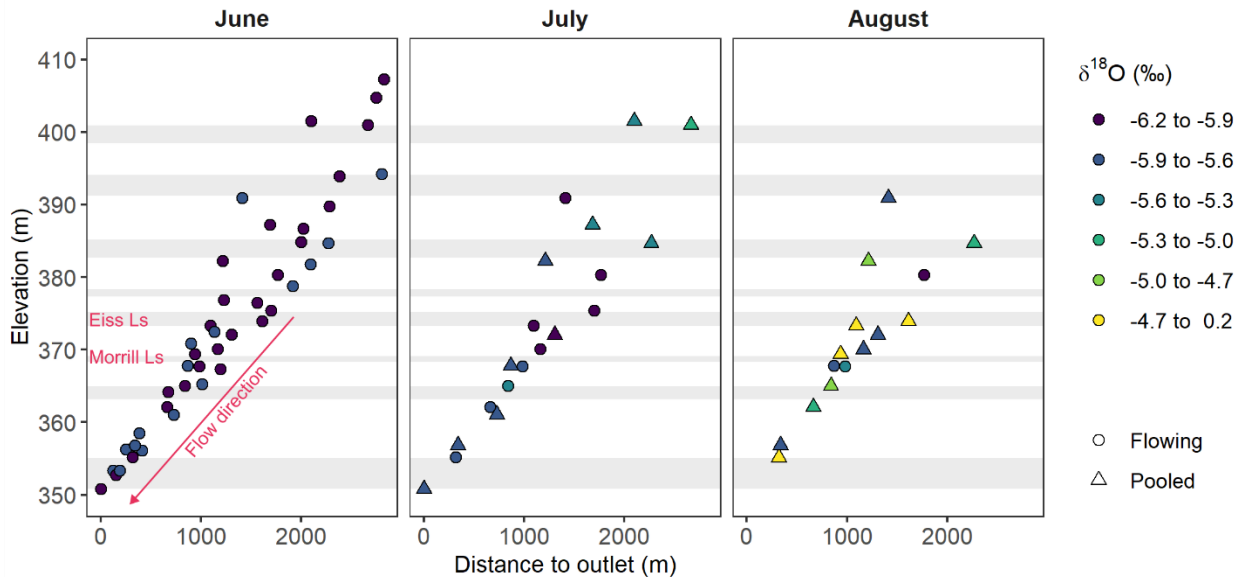
270 **3. Results & Discussion**

271 **3.1. Spatiotemporal Patterns in Stream $\delta^{18}\text{O}$ Compositions**



272
273 **Figure 3.** Spatial variation in $\delta^{18}\text{O}$ during the summer dry-down period.

274



275
276 **Figure 4.** Variation in $\delta^{18}\text{O}$ with distance to outlet during the summer dry-down period. Samples
277 collected from flowing reaches were denoted as flowing (circles), while samples taken in isolated pools
278 were considered pooled (triangles). Elevations where limestone units outcrop the watershed are shown
279 as gray bands. These elevations are based on average member thickness in the drilling log records at the
280 Konza Prairie.

281

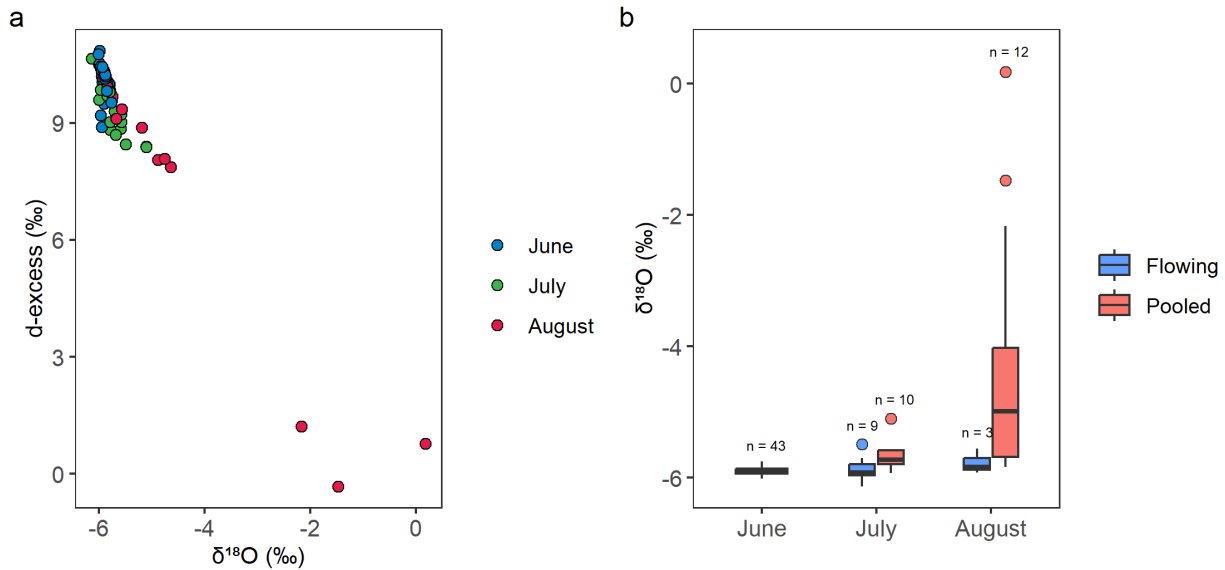
282 Over June, July, and August 2021, the South Fork of Kings Creek shifted from a fully flowing,
283 connected system to a network of isolated pools concentrated in mid-elevations (Figure 3, Figure 4). The
284 stream network went from 86% wet in June, to 38% wet in July, to 30% wet in August (Figure 3). Stream

285 network wetness was determined as the proportion of sampling sites with water present (either flowing
286 or pooled) compared to the total number of sampling sites visited. Stream drying occurred between
287 June and August at elevations below ~355m and above ~390m, while mid-elevations in the watershed
288 remained wet (Figure 4). Stream drying fragmented the network into a series of flowing reaches and
289 isolated pools, with pools representing most of the surface water in August (Figure 4). Based on past
290 studies that have linked flow to storage thresholds in the underlying limestone aquifers (Costigan et al.,
291 2015; Hatley et al., 2022). We interpret this widespread wet to dry transition as a reversal of stream-
292 aquifer gradient, whereby the stream transitioned from a net gaining condition (flow from groundwater
293 into the stream) to a net losing condition (flow from the stream into the groundwater system) during
294 the summer. However, we interpret groundwater-surface water interactions as spatially variable, and
295 localized points of drying are likely where the stream infiltrated and recharged the aquifer at that
296 location and/or upstream, while points where flow is sustained throughout the summer are likely at or
297 immediately downstream of persistent groundwater discharge points.

298 Surface water persisted at elevations in the range of several limestone aquifers, including the
299 Eiss and Morill aquifers (Figure 4). Thin 1 - 2 m karstified limestone formations throughout the
300 catchment are thought to be the primary source of water sustaining flow in the South Fork of Kings
301 Creek based on end-member mixing analysis (Hatley et al., 2022; Keen et al., 2022; Sullivan et al., 2019).
302 In the same catchments, Hatley et al. (2022) found groundwater discharge contributed > 95% of
303 streamflow during their sampling events, which spanned from April through July (2021), with minimal
304 streamflow sourced from soil water (< 1%) and direct surface runoff (< 4%). Konza's alternating
305 karstified limestone formations sustain surface water presence where they outcrop at mid-elevations in
306 the watershed during the driest parts of the year, typically late summer. Groundwater is known to
307 sustain flow in a range of systems from small headwater non-perennial streams (Hatley et al., 2022;
308 Warix et al., 2021) to large intermittent rivers (Zipper et al., 2022; Vu et al., 2018). In instances where
309 human alterations to the water cycle, e.g., groundwater pumping or surface water diversions, are
310 unimportant, such as Kings Creek, it is local groundwater and its bidirectional flow to the stream that
311 controls flow permanence and produces nuanced wetting and drying patterns in space and time
312 (Zimmer and McGlynn, 2017).

313 The $\delta^{18}\text{O}$ composition of streamwater was progressively enriched during the network dry-down
314 and variability in $\delta^{18}\text{O}$ increased considerably over the summer months (Figure 3). Stream $\delta^{18}\text{O}$ ratios in
315 the headwaters varied in space and time, ranging from -6.0‰ to -5.8 ‰ in June, -6.1‰ to -5.1‰ in July,
316 and -5.9‰ to 0.21‰ in August (Figure 3). We infer the stream to be well connected and gaining

317 groundwater from the limestone aquifers through most of the network in June, when stream $\delta^{18}\text{O}$
 318 compositions are similar across the network and the stream was flowing at all sampling points.
 319 However, as the limestone aquifers drained out in the dry summer weather and stream-aquifer
 320 gradients reversed, disparate portions of the watershed in space and time were disconnected from
 321 groundwater inputs, and the $\delta^{18}\text{O}$ signal in the remaining isolated pools became enriched due to
 322 evaporative effects.



323
 324 **Figure 5.** Variability in (a) $\delta^{18}\text{O}$ and d-excess and (b) $\delta^{18}\text{O}$ and surface water connectivity during the
 325 summer dry-down period.

326
 327 We identified two interrelated factors that influence the variation in water isotopic signatures:
 328 (1) evaporative effects, as indicated by deuterium excess (d-excess; Figure 5a) and (2) a decrease in
 329 surface water connectivity (Figure 5b). Deuterium excess (d-excess) ranged from 8.9‰ to 10.9‰ in
 330 June, 8.4‰ to 10.7‰ in July, and -0.3‰ to 10.1‰ in August (Figure 5a). Shifts to lower d-excess values
 331 are consistent with removal of light water vapor from the stream water during evaporation. Thus, the
 332 degree of evaporation-induced isotopic fractionation increased throughout the summer as conditions
 333 warmed and precipitation events became less frequent. These evaporative effects also produced
 334 differences in the $\delta^{18}\text{O}$ compositions of flowing reaches compared to isolated pools by the end of the
 335 summer (Figure 5b). Further, variability in $\delta^{18}\text{O}$ ratios increased as surface water connectivity decreased
 336 and stream-aquifer directions reversed towards losing water to the underlying limestone aquifers
 337 and/or evaporated in isolated pools above impermeable mudstones. In a random forest model to
 338 predict stream $\delta^{18}\text{O}$ during the summer months, day of year and flowing/pooled reaches were the best

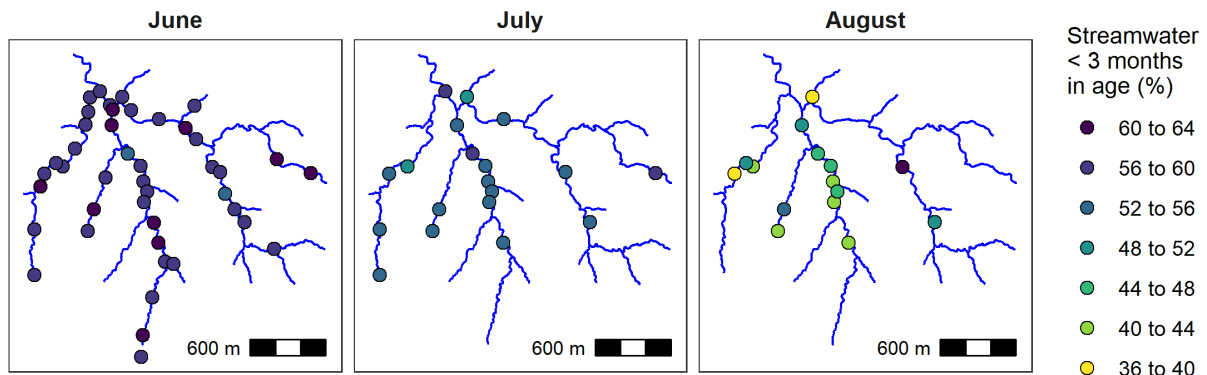
339 overall predictor for explaining observed stream $\delta^{18}\text{O}$ compositions (Figure S6), highlighting the role of
340 disconnection in driving stream water isotopic variation.

341

342 3.2. Ages and Inferred Sources of Water Sustaining Streamflow

343 3.2.1. Spatiotemporal variability during dry-down

344



345

346 **Figure 6.** Percent of streamflow less than ~3 months in age estimated from Bayesian unmixing approach.

347 Streamflow age is defined as the mean of the posterior distribution of source mixtures.

348

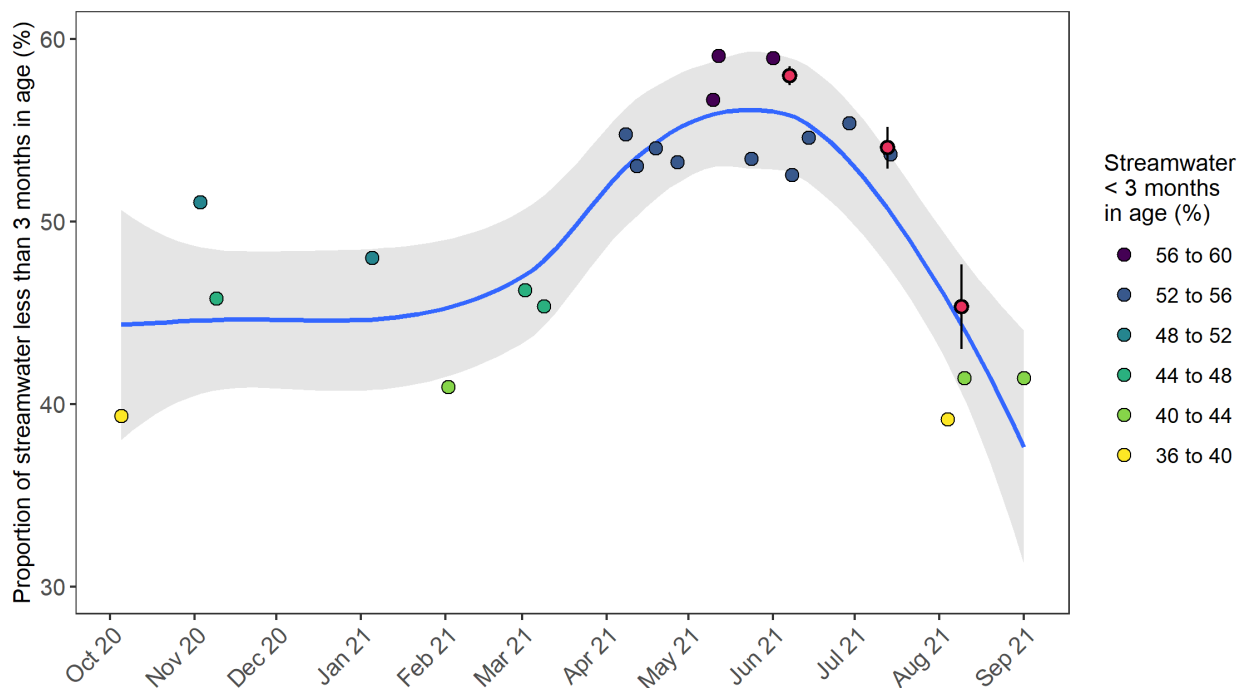
349 The age of streamflow generally became older and more spatially variable over the course of the
350 summer (Figure 6). Streamflow less than ~3 months in age ranged from 53.9% to 62.6% (mean = 58.8%)
351 during June, when the stream network was fully connected and flowing. However, as the stream
352 became disconnected, the proportion of young streamflow decreased and ranged from 49.5% to 59.0%
353 (mean = 54.0%) in July and 39.1% to 62.0% (mean = 46.4%) in August (Figure 6). We interpret these
354 results, which account for the effects of evaporation constrained by the local evaporation line and its
355 uncertainty, to reflect a shift in groundwater inputs to the stream, from fast-draining flowpaths in June
356 to more slowly draining flowpaths from lower permeability horizons later in the summer. There is
357 minimal variation in water age in June, when most of the stream network received young water from
358 recent precipitation and flow throughout the network homogenized estimated water age.

359 However, as the aquifers drained out in the dry summer weather, older water sustained flows
360 with increased variability in water age as the stream network transitioned from wet to dry and stream-
361 aquifer directions reversed so that the stream was primarily losing water to the groundwater system. In
362 July and August, the percentage of older water increased, presumably from water with more varied age
363 compositions being transported through less permeable pore space and reduced mixing due to
364 decreased surface water connectivity (Figure 4), though network-wide approximately half of the stream

365 water was still younger than 3 months in age. The high percentage of young water aligns with past
366 studies that have shown preferential flow (i.e., soil macropores, fractures, solution-enlarged pores, and
367 springs) to be important in this watershed, as these flowpaths can quickly route water to the stream
368 (Macpherson and Sullivan, 2019; Tsy-pin and Macpherson, 2012; Macpherson et al., 2008). Similarly high
369 young water fractions (reaching up to 40%) and short mean transit times (0.34 to 0.74 years) have been
370 reported in other small headwater non-perennial streams in karst aquifers, where young water is likely
371 transmitted via well-developed karst conduits (Rusjan et al., 2019).

372

373 3.2.2. Implications at watershed outlet



374

375 **Figure 7.** Streamflow less than ~3 months in age from Bayesian unmixing at the NEON sampling site. For
376 comparison, the red dots show the average and 95% confidence interval of all the synoptic sampling
377 points (i.e., all points in Figure 3). The blue line and shaded interval show a loess fit with its 95%
378 confidence interval for the Bayesian unmixing of the NEON sampling site.

379

380 Streamflow at the catchment outlet was younger when the network was fully-connected and
381 flowing, and became older and temporally variable as the network transitioned to a state of drying
382 (Figure 7). Streamflow less than ~3 months in age ranged from 39.2% to 59.1% in 2021, with older water
383 sustaining streamflows during the driest parts of the year in later summer, fall, and winter. The age of

384 streamflow at the catchment outlet followed the same trajectory as in the headwaters, and thus we
385 observed good agreement in water age estimates between the Bayesian unmixing of the synoptic
386 samples and the downstream NEON samples. We interpret the combined spatial and temporal evolution
387 of water age to suggest a shift away from rapid fracture flow towards slower matrix flow that creates a
388 sustained but localized surface water presence during the driest parts of the year that is mirrored in
389 both the headwaters and at the outlet.

390

391 **3.3 Synthesizing evidence of water age and source in non-perennial streams**

392 Multiple studies have concluded that groundwater sustains flow in the South Fork of Kings Creek
393 (Hatley et al., 2022; Keen et al., 2022; Sullivan et al., 2019); however, the transit time for groundwater to
394 reach the stream remained unknown. We found the South Fork of Kings Creek shifted from a fully
395 flowing, connected system to a network of isolated pools, where surface water persisted due to
396 groundwater inputs from the many limestone aquifers (Figure 3 and 4). During the network dry-down,
397 the $\delta^{18}\text{O}$ composition of streamwater was progressively enriched due to evaporative effects and a
398 decrease in surface water connectivity (Figure 5). Multiple lines of evidence suggest that a substantial
399 amount of summer streamflow (up to 62.6% at points) originated as young water sourced from spring
400 rains and high-intensity summer storms (Figure 6 and 7).

401 Streamflow in the South Fork of Kings Creek and at the outlet is a mixture of young and old
402 water, with increasing age as the stream network dries, indicating that old water can be stored in the
403 subsurface but remain disconnected from the stream for part of the year. Understanding this mixture of
404 young and old water in generating streamflow provides another line of evidence for the “fill and spill”
405 hydrology hypothesized to operate in the Konza Prairie and other similar merokarst settings, where
406 storage thresholds control flow permanence (Costigan et al., 2015; McDonnell et al., 2021). In brief,
407 when the watershed is dry, precipitation infiltrates into the subsurface to “fill” the many limestone
408 aquifers, but does not push groundwater to the stream. However, as the limestone aquifers exceed
409 some critical threshold of storage, they “spill” by pushing groundwater to the stream. At the point when
410 storage thresholds are exceeded, precipitation and streamflow patterns are synchronized, meaning that
411 discharge tends to increase contemporaneously with precipitation events, ultimately recoupling the
412 hydrologic flow regime of the stream to sub-annual weather patterns (Costigan et al., 2015). For
413 instance, we observed the onset of fill to end of spill, where it rained above average in March (81.5
414 percentile of 30 year conditions), but this precipitation did not generate streamflow until the limestone
415 aquifers had “filled” by the start of April, representing a period of time when precipitation and

416 streamflow patterns were desynchronized (Figure 2). Our results suggest that spring and early summer
417 rains provided a substantial flux of young water that was transmitted to the underlying limestone
418 aquifers through soil macropores and bedrock fractures (noted in Macpherson and Sullivan, 2019;
419 Tsy-pin and Macpherson, 2012; Macpherson et al., 2008) and, once storage thresholds were exceeded,
420 the stream network transitioned to flowing and connected, recoupling the response of streamflow to
421 precipitation. As the stream dried, the shift in water age indicates a shift in water sources from within-
422 year preferential groundwater discharge to much older groundwater that was pushed out of less
423 permeable matrix pore space. Taken together, our study indicates that seasonal contributions of young
424 water drive storage above critical thresholds causing wet-up, while old water is more slowly pushed out
425 of the less permeable pore space thereby sustaining surface water during the driest parts of summer.

426

427 **3.4 Implications for water management and policy**

428 Non-perennial streams are the source of considerable policy and management debate; in the
429 US, much of the debate centers on their connection to downstream sources (see Section 1). Thus, our
430 demonstration of the prevalence of relatively fast flowpaths in sustaining flow in non-perennial streams
431 provides a structural “significant nexus” between activities on the landscape, non-perennial headwater
432 streams, and their downstream perennial rivers in merokarst regions. Therefore, our results suggest that
433 management decisions that impair water quality and/or quantity in non-perennial watersheds have the
434 potential to “significantly affect the chemical, physical, and biological integrity” of downstream
435 navigable waters (Clean Water Rule, 2015). Due to the predominance of fast flowpaths sustaining
436 streamflow in Kings Creek, nutrients and contaminants have the potential to be transported over short
437 timescales from the landscape to the stream, with little time for attenuation.

438 These fast flowpaths may exert a disproportionate influence on downstream water quality. For
439 example, in agricultural regions, nitrate from farming operations has extensively degraded surface and
440 groundwater quality; the prevalence of fast groundwater flowpaths in regions with high legacy nitrogen
441 load could contribute to on-going declines in surface water quality (Byrnes et al., 2020; Van Meter et al.,
442 2018; Van Meter et al., 2016). As another example, even much longer groundwater flowpaths have been
443 shown to transport contaminants over sub-annual timescales (< 10 months), as seen in the contentious
444 County of Maui, Hawaii v. Hawaii Wildlife Fund case (Cornwall, 2020; Craig et al., 2013). Degradation of
445 water quality could be further compounded by changes in water availability driven by short-term
446 hydroclimatic change and longer-term changes in groundwater dynamics, which could cause
447 downstream perennial waters to receive increasingly variable streamflows, with potential to affect our

448 ability to meet both agricultural and domestic water requirements. These climate-driven changes may
449 be compounded by modifications to land use, such as urbanization that can alter partitioning of water
450 between runoff and groundwater recharge (Zipper et al., 2017), deforestation for agricultural expansion
451 that can increase groundwater levels (Gimenez et al., 2016), or woody vegetation encroachment which
452 can decrease recharge in grasslands (Keen et al., 2022). Indeed, given the potential for climate and land
453 use-driven changes to hydrology, policymakers and water managers may need to account for the
454 potential fast transit of water from the landscape to non-perennial streams to downstream perennial
455 waters.

456

457 **4. Conclusions**

458 We used water isotopes with a Bayesian unmixing approach to partition water age, water
459 source, and associated changes during the summer dry-down of a non-perennial headwater stream
460 network at the Konza Prairie. We found pronounced spatial and temporal variability in stream $\delta^{18}\text{O}$
461 compositions during the summer dry-down period due to evaporative effects and a decrease in surface
462 water connectivity. Water age estimates from two independent datasets are similar, suggesting that our
463 Bayesian Unmixing approach is a useful method for understanding water age at multiple points in a
464 watershed when streamwater isotope data span less than a year. We found that a substantial amount of
465 streamflow in the South Fork of Kings Creek originated as young water sourced from within-season
466 precipitation that had been stored in the subsurface for less than ~3 months, regardless of position in
467 the watershed. As the summer progressed, there was a shift to older water sources, with variability in
468 age compositions distributed throughout the drying stream network. We interpret this water age
469 transition as a shift in water source towards less permeable and slower subsurface flowpaths that
470 sustain flow during the driest parts of the year. The predominance of young water routed along fast
471 flowpaths suggests a rapid connection between these upstream headwaters to downstream perennial
472 waters, indicating that changes to water quality and/or quantity in non-perennial streams have the
473 potential to cause significant downstream consequences.

474

475 **Acknowledgments**

476 We thank all collaborators on Aquatic Intermittency Effects of Microbiomes in Streams (AIMS) who
477 assisted in the synoptic sampling campaigns, as well as the Konza Prairie Biological Station and its staff
478 for site access and management. Specifically, we thank Sarah Flynn, Simmi Rana, Jessica Wilhelm,
479 Michelle Wolford and Kaci Zarek for the additional sample collection field work in July and August.

480 Additionally, we would like to thank the National Ecological Observatory Network and the Konza Prairie
481 Long Term Ecological Research programs for their long-term data collection efforts which supported our
482 analysis, and conversations with Gwen MacPherson and Walter Dodds on the hydrology of Konza.
483 Support was provided by a National Science Foundation awards OIA-2019603 and DEB-2025849.

484

485 **Open Research**

486 The data and scripts associated with this study are available in the Zenodo repository at:

487 <https://doi.org/10.5281/zenodo.7633403>

488

489 **References**

490 Alexander, L. C. (2015). Science at the boundaries: scientific support for the Clean Water Rule.

491 *Freshwater Science*, 34(4), 1588–1594. <https://doi.org/10.1086/684076>

492 Allen, D. C., Datry, T., Boersma, K. S., Bogan, M. T., Boulton, A. J., Bruno, D., et al. (2020). River

493 ecosystem conceptual models and non-perennial rivers: A critical review. *WIREs Water*, 7(5),

494 e1473. <https://doi.org/10.1002/wat2.1473>

495 Barry, E. (2018). Characterizing groundwater flow through merokarst, northeast, Kansas, USA (MS

496 thesis). University of Kansas.

497 Benettin, P., Rodriguez, N. B., Sprenger, M., Kim, M., Klaus, J., Harman, C. J., et al. (2022). Transit

498 Time Estimation in Catchments: Recent Developments and Future Directions. *Water Resources*

499 *Research*, 58(11), e2022WR033096. <https://doi.org/10.1029/2022WR033096>

500 Botter, G., & Durighetto, N. (2020). The Stream Length Duration Curve: A Tool for Characterizing

501 the Time Variability of the Flowing Stream Length. *Water Resources Research*, 56(8),

502 e2020WR027282. <https://doi.org/10.1029/2020WR027282>

503 Bowen, G. J. (2022). isoWater: Discovery, retrieval, and analysis of water isotope data (Version

504 1.1.1). Retrieved from <https://CRAN.R-project.org/package=isoWater>

505 Bowen, G. J., Putman, A., Brooks, J. R., Bowling, D. R., Oerter, E. J., & Good, S. P. (2018). Inferring

506 the source of evaporated waters using stable H and O isotopes. *Oecologia*, 187(4), 1025–1039.

507 <https://doi.org/10.1007/s00442-018-4192-5>

508 Brookfield, A. e., Macpherson, G. I., & Covington, M. d. (2017). Effects of Changing Meteoric

509 Precipitation Patterns on Groundwater Temperature in Karst Environments. *Groundwater*,

510 55(2), 227–236. <https://doi.org/10.1111/gwat.12456>

511 Busch, M. H., Costigan, K. H., Fritz, K. M., Datry, T., Krabbenhoft, C. A., Hammond, J. C., et al. (2020).
512 What's in a Name? Patterns, Trends, and Suggestions for Defining Non-Perennial Rivers and
513 Streams. *Water*, 12(7), 1980. <https://doi.org/10.3390/w12071980>

514 Byrnes, D. K., Van Meter, K. J., & Basu, N. B. (2020). Long-Term Shifts in U.S. Nitrogen Sources and
515 Sinks Revealed by the New TREND-Nitrogen Data Set (1930–2017). *Global Biogeochemical*
516 *Cycles*, 34(9), e2020GB006626. <https://doi.org/10.1029/2020GB006626>

517 Clean Water Rule: Definition of “Waters of the United States.” (2015, June 29). Retrieved from
518 [https://www.federalregister.gov/documents/2015/06/29/2015-13435/clean-water-rule-](https://www.federalregister.gov/documents/2015/06/29/2015-13435/clean-water-rule-definition-of-waters-of-the-united-states)
519 [definition-of-waters-of-the-united-states](https://www.federalregister.gov/documents/2015/06/29/2015-13435/clean-water-rule-definition-of-waters-of-the-united-states)

520 Cornwall, W. (2020, April 23). ‘Hydrologists should be happy.’ Big Supreme Court ruling bolsters
521 groundwater science. *Science*. Retrieved from
522 <https://www.science.org/content/article/scotus-clean-water>

523 Costigan, K. H., Daniels, M. D., & Dodds, W. K. (2015). Fundamental spatial and temporal
524 disconnections in the hydrology of an intermittent prairie headwater network. *Journal of*
525 *Hydrology*, 522, 305–316. <https://doi.org/10.1016/j.jhydrol.2014.12.031>

526 Costigan, K. H., Jaeger, K. L., Goss, C. W., Fritz, K. M., & Goebel, P. C. (2016). Understanding controls
527 on flow permanence in intermittent rivers to aid ecological research: integrating meteorology,
528 geology and land cover. *Ecohydrology*, 9(7), 1141–1153. <https://doi.org/10.1002/eco.1712>

529 Craig, H. (1961). Isotopic Variations in Meteoric Waters. *Science*, 133(3465), 1702–1703.
530 <https://doi.org/10.1126/science.133.3465.1702>

531 Dansgaard, W. (1964). Stable isotopes in precipitation. *Tellus*, 16(4), 436–468.
532 <https://doi.org/10.1111/j.2153-3490.1964.tb00181.x>

533 Datry, T., Truchy, A., Olden, J. D., Busch, M. H., Stubbington, R., Dodds, W. K., et al. (2023). Causes,
534 Responses, and Implications of Anthropogenic versus Natural Flow Intermittence in River
535 Networks. *BioScience*, 73(1), 9–22. <https://doi.org/10.1093/biosci/biac098>

536 Giménez, R., Mercau, J., Noretto, M., Páez, R., & Jobbágy, E. (2016). The ecohydrological imprint of
537 deforestation in the semiarid Chaco: insights from the last forest remnants of a highly
538 cultivated landscape. *Hydrological Processes*, 30(15), 2603–2616.
539 <https://doi.org/10.1002/hyp.10901>

540 Glenn, C. R., Whittier, R. B., Dailer, M. L., Dulaiova, H., El-Kadi, A. I., Fackrell, J., et al. (2013). Lahaina
541 groundwater tracer study -- Lahaina, Maui, Hawaii. Retrieved from
542 <http://hdl.handle.net/10125/50768>

543 Gómez, R., Arce, M. I., Baldwin, D. S., & Dahm, C. N. (2017). Chapter 3.1 - Water Physicochemistry
544 in Intermittent Rivers and Ephemeral Streams. In T. Datry, N. Bonada, & A. Boulton (Eds.),
545 *Intermittent Rivers and Ephemeral Streams* (pp. 109–134). Academic Press.
546 <https://doi.org/10.1016/B978-0-12-803835-2.00005-X>

547 Hale, R. L., & Godsey, S. E. (2019). Dynamic stream network intermittence explains emergent
548 dissolved organic carbon chemostasis in headwaters. *Hydrological Processes*, 33(13), 1926–
549 1936. <https://doi.org/10.1002/hyp.13455>

550 Harman, C. J. (2015). Time-variable transit time distributions and transport: Theory and application
551 to storage-dependent transport of chloride in a watershed. *Water Resources Research*, 51(1),
552 1–30. <https://doi.org/10.1002/2014WR015707>

553 Hatley, C. M., Armijo, B., Andrews, K., Anhold, C., Nippert, J. B., & Kirk, M. F. (2023). Intermittent
554 streamflow generation in a merokarst headwater catchment. *Environmental Science:
555 Advances*, 2(1), 115–131. <https://doi.org/10.1039/D2VA00191H>

556 Hayden, B. P. (n.d.). Regional climate and the distribution of tallgrass prairie. In A. K. Knapp, J. M.
557 Briggs, D. C. Hartnett, & S. L. Collins (Eds.), *Grassland Dynamics* (pp. 19–34). New York: Oxford
558 University Press.

559 Hrachowitz, M., Benettin, P., van Breukelen, B. M., Fovet, O., Howden, N. J. K., Ruiz, L., et al. (2016).
560 Transit times—the link between hydrology and water quality at the catchment scale. *WIREs
561 Water*, 3(5), 629–657. <https://doi.org/10.1002/wat2.1155>

562 Jasechko, S. (2019). Global Isotope Hydrogeology—Review. *Reviews of Geophysics*, 57(3), 835–965.
563 <https://doi.org/10.1029/2018RG000627>

564 Jensen, C. K., McGuire, K. J., McLaughlin, D. L., & Scott, D. T. (2019). Quantifying spatiotemporal
565 variation in headwater stream length using flow intermittency sensors. *Environmental
566 Monitoring and Assessment*, 191(4), 226. <https://doi.org/10.1007/s10661-019-7373-8>

567 Keen, R. M., Nippert, J. B., Sullivan, P. L., Ratajczak, Z., Ritchey, B., O’Keefe, K., & Dodds, W. K.
568 (2022). Impacts of Riparian and Non-riparian Woody Encroachment on Tallgrass Prairie
569 Ecohydrology. *Ecosystems*. <https://doi.org/10.1007/s10021-022-00756-7>

570 Kirchner, J. W. (2016a). Aggregation in environmental systems Part 1: Seasonal tracer cycles
571 quantify young water fractions, but not mean transit times, in spatially heterogeneous
572 catchments. *Hydrology and Earth System Sciences*, 20(1), 279–297.
573 <https://doi.org/10.5194/hess-20-279-2016>

574 Klaus, J., & McDonnell, J. J. (2013). Hydrograph separation using stable isotopes: Review and
575 evaluation. *Journal of Hydrology*, 505, 47–64. <https://doi.org/10.1016/j.jhydrol.2013.09.006>

576 Krabbenhoft, C. A., Allen, G. H., Lin, P., Godsey, S. E., Allen, D. C., Burrows, R. M., et al. (2022).
577 Assessing placement bias of the global river gauge network. *Nature Sustainability*, 5(7), 586–
578 592. <https://doi.org/10.1038/s41893-022-00873-0>

579 Leone, M., Gentile, F., Lo Porto, A., Ricci, G. F., & De Girolamo, A. M. (2023). Ecological flow in
580 southern Europe: Status and trends in non-perennial rivers. *Journal of Environmental*
581 *Management*, 342, 118097. <https://doi.org/10.1016/j.jenvman.2023.118097>

582 Liptak, A. (2023, May 25). Supreme Court Limits E.P.A.'s Power to Address Water Pollution. The
583 New York Times. Retrieved from [https://www.nytimes.com/2023/05/25/us/supreme-court-](https://www.nytimes.com/2023/05/25/us/supreme-court-epa-water-pollution.html)
584 [epa-water-pollution.html](https://www.nytimes.com/2023/05/25/us/supreme-court-epa-water-pollution.html)

585 Macpherson, G. L. (1996). Hydrogeology of thin limestones: the Konza Prairie Long-Term Ecological
586 Research Site, Northeastern Kansas. *Journal of Hydrology*, 186(1), 191–228.
587 [https://doi.org/10.1016/S0022-1694\(96\)03029-6](https://doi.org/10.1016/S0022-1694(96)03029-6)

588 Macpherson, G. L., & Sullivan, P. L. (2019). Watershed-scale chemical weathering in a merokarst
589 terrain, northeastern Kansas, USA. *Chemical Geology*, 527, 118988.
590 <https://doi.org/10.1016/j.chemgeo.2018.12.001>

591 Macpherson, G. L., Roberts, J. A., Blair, J. M., Townsend, M. A., Fowle, D. A., & Beisner, K. R. (2008).
592 Increasing shallow groundwater CO₂ and limestone weathering, Konza Prairie, USA.
593 *Geochimica et Cosmochimica Acta*, 72(23), 5581–5599.
594 <https://doi.org/10.1016/j.gca.2008.09.004>

595 Maher, K. (2010). The dependence of chemical weathering rates on fluid residence time. *Earth and*
596 *Planetary Science Letters*, 294(1), 101–110. <https://doi.org/10.1016/j.epsl.2010.03.010>

597 McDonnell, J. J., Spence, C., Karran, D. J., van Meerveld, H. J. (Ilja), & Harman, C. J. (2021). Fill-and-
598 Spill: A Process Description of Runoff Generation at the Scale of the Beholder. *Water*
599 *Resources Research*, 57(5), e2020WR027514. <https://doi.org/10.1029/2020WR027514>

600 Messager, M. L., Lehner, B., Cockburn, C., Lamouroux, N., Pella, H., Snelder, T., et al. (2021). Global
601 prevalence of non-perennial rivers and streams. *Nature*, 594(7863), 391–397.
602 <https://doi.org/10.1038/s41586-021-03565-5>

603 Meter, K. J. V., Basu, N. B., Veenstra, J. J., & Burras, C. L. (2016). The nitrogen legacy: emerging
604 evidence of nitrogen accumulation in anthropogenic landscapes. *Environmental Research*
605 *Letters*, 11(3), 035014. <https://doi.org/10.1088/1748-9326/11/3/035014>

606 National Ecological Observatory Network (NEON). (2022a). Stable isotopes in precipitation
607 (DP1.00038.001). National Ecological Observatory Network (NEON).
608 <https://doi.org/10.48443/E3MY-7V57>

609 National Ecological Observatory Network (NEON). (2022b). Stable isotopes in surface water
610 (DP1.20206.001). National Ecological Observatory Network (NEON).
611 <https://doi.org/10.48443/YZ7H-F560>

612 The Navigable Waters Protection Rule: Definition of “Waters of the United States.” (2020, April 21).
613 Retrieved from [https://www.federalregister.gov/documents/2020/04/21/2020-02500/the-](https://www.federalregister.gov/documents/2020/04/21/2020-02500/the-navigable-waters-protection-rule-definition-of-waters-of-the-united-states)
614 [navigable-waters-protection-rule-definition-of-waters-of-the-united-states](https://www.federalregister.gov/documents/2020/04/21/2020-02500/the-navigable-waters-protection-rule-definition-of-waters-of-the-united-states)

615 Nippert, J. (2022). AWEOL Meteorological data from the Konza prairie headquarters weather station.
616 Environmental Data Initiative. Retrieved from
617 <http://dx.doi.org/10.6073/pasta/98b9d0a612c17ab9f8f121d9741e72a6>

618 Pomes, M. (1995). A study of the aquatic humic substances and hydrogeology in a prairie
619 watershed: Use of humic material as a tracer of recharge through soils (PhD thesis). University
620 of Kansas.

621 Price, A. N., Jones, C. N., Hammond, J. C., Zimmer, M. A., & Zipper, S. C. (2021). The Drying Regimes
622 of Non-Perennial Rivers and Streams. *Geophysical Research Letters*, 48(14), e2021GL093298.
623 <https://doi.org/10.1029/2021GL093298>

624 Ransom, M. D., Rice, C. W., & Todd, T. C. (n.d.). Soils and soil biota. In A. K. Knapp, J. M. Briggs, D. C.
625 Hartnett, & S. L. Collins (Eds.), *Grassland Dynamics: Long-term ecological research in tallgrass*
626 *prairie* (pp. 48–66). New York: Oxford University Press.

627 Revised Definition of “Waters of the United States.” (2023, January 18). Retrieved from
628 [https://www.federalregister.gov/documents/2023/01/18/2022-28595/revised-definition-of-](https://www.federalregister.gov/documents/2023/01/18/2022-28595/revised-definition-of-waters-of-the-united-states)
629 [waters-of-the-united-states](https://www.federalregister.gov/documents/2023/01/18/2022-28595/revised-definition-of-waters-of-the-united-states)

630 Rusjan, S., Sapač, K., Petrič, M., Lojen, S., & Bezak, N. (2019). Identifying the hydrological behavior
631 of a complex karst system using stable isotopes. *Journal of Hydrology*, 577, 123956.
632 <https://doi.org/10.1016/j.jhydrol.2019.123956>

633 Shanafield, M., Bourke, S. A., Zimmer, M. A., & Costigan, K. H. (2021). An overview of the hydrology
634 of non-perennial rivers and streams. *WIREs Water*, 8(2), e1504.
635 <https://doi.org/10.1002/wat2.1504>

636 Sullivan, P. L., Stops, M. W., Macpherson, G. L., Li, L., Hirmas, D. R., & Dodds, W. K. (2019). How
637 landscape heterogeneity governs stream water concentration-discharge behavior in carbonate

638 terrains (Konza Prairie, USA). *Chemical Geology*, 527, 118989.
639 <https://doi.org/10.1016/j.chemgeo.2018.12.002>

640 Sullivan, Pamela L., Zhang, C., Behm, M., Zhang, F., & Macpherson, G. L. (2020). Toward a new
641 conceptual model for groundwater flow in merokarst systems: Insights from multiple
642 geophysical approaches. *Hydrological Processes*, 34(24), 4697–4711.
643 <https://doi.org/10.1002/hyp.13898>

644 Swenson, L. J., Zipper, S., Peterson, D. M., Jones, C. N., Burgin, A. J., Seybold, E., Kirk, M.F., Hatley,
645 C. (2023). Water isotopes and associated scripts for the analysis of water age and source.
646 [Dataset]. Zenodo. <https://doi.org/10.5281/zenodo.7633403>

647 Trambly, Y., Rutkowska, A., Sauquet, E., Sefton, C., Laaha, G., Osuch, M., et al. (2021). Trends in
648 flow intermittence for European rivers. *Hydrological Sciences Journal*, 66(1), 37–49.
649 <https://doi.org/10.1080/02626667.2020.1849708>

650 Tsy-pin, M., & Macpherson, G. L. (2012). The effect of precipitation events on inorganic carbon in
651 soil and shallow groundwater, Konza Prairie LTER Site, NE Kansas, USA. *Applied Geochemistry*,
652 27(12), 2356–2369. <https://doi.org/10.1016/j.apgeochem.2012.07.008>

653 Van Meter, K. J., Van Cappellen, P., & Basu, N. B. (2018). Legacy nitrogen may prevent achievement
654 of water quality goals in the Gulf of Mexico. *Science*, 360(6387), 427–430.
655 <https://doi.org/10.1126/science.aar4462>

656 Vero, S. e., Macpherson, G. I., Sullivan, P. I., Brookfield, A. e., Nippert, J. b., Kirk, M. f., et al. (2018).
657 Developing a Conceptual Framework of Landscape and Hydrology on Tallgrass Prairie:A Critical
658 Zone Approach. *Vadose Zone Journal*, 17(1), 170069. <https://doi.org/10.2136/vzj2017.03.0069>

659 Vu, H. M., Shanafield, M., & Batelaan, O. (2018). Flux dynamics at the groundwater-surface water
660 interface in a tropical catchment. *Limnologica*, 68, 36–45.
661 <https://doi.org/10.1016/j.limno.2017.06.003>

662 Walsh, R., & Ward, A. S. (2022). An overview of the evolving jurisdictional scope of the U.S. Clean
663 Water Act for hydrologists. *WIREs Water*, 9(5), e1603. <https://doi.org/10.1002/wat2.1603>

664 Ward, A. S., Wade, J., Kelleher, C., & Schewe, R. L. (2023). Clarify jurisdiction of US Clean Water Act.
665 *Science*, 379(6628), 148–148. <https://doi.org/10.1126/science.adf7391>

666 Warix, S. R., Godsey, S. E., Lohse, K. A., & Hale, R. L. (2021). Influence of groundwater and
667 topography on stream drying in semi-arid headwater streams. *Hydrological Processes*, 35(5),
668 e14185. <https://doi.org/10.1002/hyp.14185>

669 Xia, C., Zuecco, G., Chen, K., Liu, L., Zhang, Z., & Luo, J. (2023). The estimation of young water
670 fraction based on isotopic signals: challenges and recommendations. *Frontiers in Ecology and*
671 *Evolution*, 11. Retrieved from
672 <https://www.frontiersin.org/articles/10.3389/fevo.2023.1114259>

673 Zarnetske, J. P., Haggerty, R., Wondzell, S. M., & Baker, M. A. (2011). Dynamics of nitrate
674 production and removal as a function of residence time in the hyporheic zone. *Journal of*
675 *Geophysical Research: Biogeosciences*, 116(G1). <https://doi.org/10.1029/2010JG001356>

676 Zimmer, M. A., & McGlynn, B. L. (2017). Bidirectional stream–groundwater flow in response to
677 ephemeral and intermittent streamflow and groundwater seasonality. *Hydrological Processes*,
678 31(22), 3871–3880. <https://doi.org/10.1002/hyp.11301>

679 Zimmer, M. A., & McGlynn, B. L. (2018). Lateral, Vertical, and Longitudinal Source Area Connectivity
680 Drive Runoff and Carbon Export Across Watershed Scales. *Water Resources Research*, 54(3),
681 1576–1598. <https://doi.org/10.1002/2017WR021718>

682 Zimmer, M. A., Burgin, A. J., Kaiser, K., & Hosen, J. (2022). The unknown biogeochemical impacts of
683 drying rivers and streams. *Nature Communications*, 13(1), 7213.
684 <https://doi.org/10.1038/s41467-022-34903-4>

685 Zipper, S. C., Soylyu, M. E., Kucharik, C. J., & Loheide II, S. P. (2017). Quantifying indirect
686 groundwater-mediated effects of urbanization on agroecosystem productivity using
687 MODFLOW-AgroIBIS (MAGI), a complete critical zone model. *Ecological Modelling*, 359, 201–
688 219. <https://doi.org/10.1016/j.ecolmodel.2017.06.002>

689 Zipper, S., Popescu, I., Compare, K., Zhang, C., & Seybold, E. C. (2022). Alternative stable states and
690 hydrological regime shifts in a large intermittent river. *Environmental Research Letters*, 17(7),
691 074005. <https://doi.org/10.1088/1748-9326/ac7539>

692 Zipper, S. C., Hammond, J. C., Shanafield, M., Zimmer, M., Datry, T., Jones, C. N., et al. (2021).
693 Pervasive changes in stream intermittency across the United States. *Environmental Research*
694 *Letters*, 16(8), 084033. <https://doi.org/10.1088/1748-9326/ac14ec>



PUBLICATIONS

695

696

Water Resources Research

697

Supporting Information for

698

Changes in water age during dry-down of a non-perennial stream

699 Logan J. Swenson^{1,2,*}, Sam Zipper¹, Delaney M. Peterson³, C. Nathan Jones³, Amy J. Burgin⁴, Erin
700 Seybold¹, Matthew F. Kirk⁵, Camden Hatley^{1,2}

701

1. Kansas Geological Survey, University of Kansas

702

2. Department of Geology, University of Kansas

703

3. Department of Biological Sciences, University of Alabama

704

4. Kansas Biological Survey-Center for Ecological Research, University of Kansas

705

5. Department of Geology, Kansas State University

706

Corresponding author: loganswenson@ku.edu

707

Contents of this file

708

709

Text S1 and S2

710

Figures S1 to S6

711

Introduction

712

This SI contains a detailed description of our sampling strategy (Text S1), random forest to

713

predict $\delta^{18}\text{O}$ compositions (Text S2), and supplementary figures (Figures S1 to S6).

714

715

716

717

718

719 **Text S1. Sampling strategy**

720 The 50 sampling sites in this study were defined to leverage existing long-term data while
721 spanning a range of watershed physiographic and no-flow conditions. In addition to the water
722 isotope samples investigated in this study, these sampling sites were also used for a variety of
723 other samples including microbial and macroinvertebrate communities, other water chemistry
724 parameters, and instrumentation with stream temperature, intermittency, and conductivity (STIC)
725 sensors, and therefore the sampling approach used was meant to balance the competing
726 priorities of these teams, rather than optimize the sampling from a purely isotope-driven
727 perspective.

728 First, we identified a subset of priority locations that we wanted to ensure were sampled.
729 These priority locations included sites with existing hydrological data including long-term weirs
730 maintained by the Konza LTER network (n=4), existing stream intermittency sensors from other
731 projects (n=10, which included our planned watershed outlet location), locations immediately
732 downstream of a subset of springs identified during field mapping campaigns (n=7), and near
733 unmonitored tributary junctions (n=2). Combined, these priority locations made up 23 of our
734 sampling sites.

735 For the remaining 27 sites, we distributed sampling sites using a stratified random
736 sampling approach spanning two variables that have previously been shown to influence stream
737 intermittency: topographic wetness index (TWI) and drainage area (Warix et al., 2021). TWI is a
738 unitless physiographic variable that integrates drainage area and local slope, and locations with
739 higher TWI values are locations that may be wetter due to the accumulation of water from
740 upslope areas. To distribute the points randomly, we first discretized the stream network into
741 equally spaced points at 2 m resolution, which matches the resolution of the DEM used to create
742 the stream network map. We then binned these points into 10 bins that had approximately
743 equal width at the lower end of the drainage area distribution, where points were more densely
744 concentrated, and approximately the same number of total stream points at the higher end of
745 the drainage area distribution, where points were less densely concentrated (Figure S1).

746 To obtain 50 total sampling points spanning a range of TWI and drainage area conditions,
747 we attempted to place 5 sampling sites within each drainage area bin that spanned the range of
748 TWI values within that bin. To accomplish this, for each drainage area bin we split the range of
749 TWI into 5 quantiles, which we refer to here as bin-quantiles. We identified how many priority
750 locations were already within each bin-quantile and randomly selected a point on the stream
751 network within each bin-quantile, ensuring that it was > 100 m from any existing sampling site.
752 If the priority sites included multiple sampling sites within a given bin-quantile, we could not
753 place a sampling site in each of the bin-quantiles, in which case we randomly selected bin-
754 quantiles to reach a total of 5 sampling sites within that drainage area bin. There were 6 bin-
755 quantiles that we were unable to select sampling sites because all points within that bin-quantile
756 were within 100 m of an existing sampling site. These remaining 6 sampling sites were placed by
757 manually inspecting the stream network and identifying substantial gaps. We then made slight
758 adjustments to some of the sampling sites that were randomly located, for example moving the
759 location from downstream to upstream of a road crossing and/or further back from a tributary
760 junction.

761 The final distribution of the 50 sampling sites with respect to drainage area and TWI is
762 shown in Figure S2 and Figure S3. Figure 1 shows the spatial distribution of the sampling sites
763 within the stream network.

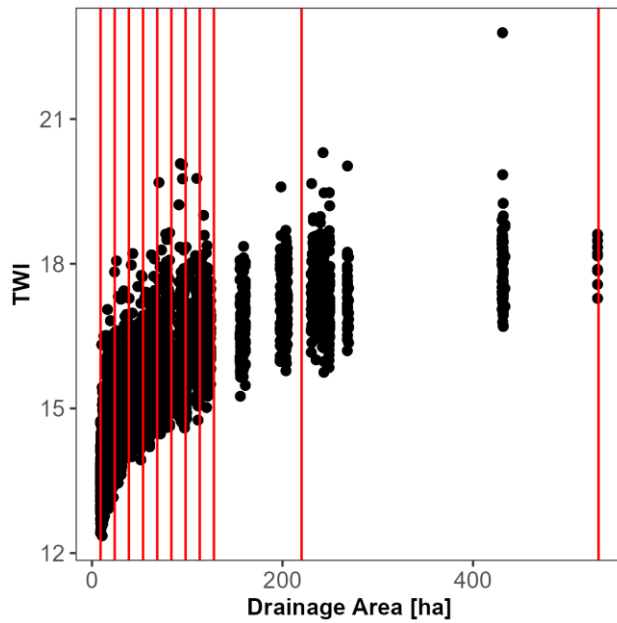
764 **Text S2. Random forest to predict $\delta^{18}\text{O}$ compositions**

765 We developed a random forest model to predict stream $\delta^{18}\text{O}$ ratios and to quantify the
766 factors that most strongly influence $\delta^{18}\text{O}$ during the summer dry-down of the South Fork of
767 Kings Creek (i.e., the synoptic samples only) using the *party* package in R (Hothorn et al., 2006;
768 Strobl et al., 2007; Strobl et al., 2008). Random forest models are particularly well-suited for
769 hydrological prediction due to their ability to handle numerous predictors with potentially
770 nonlinear and interacting relationships, relatively low risk of overfitting, and ease in interpreting
771 the importance of each input variable (Eng et al., 2017; Addor et al., 2018; Miller et al., 2018). We
772 developed a random forest model to predict $\delta^{18}\text{O}$ across all sites and sampling dates using the
773 following predictor variables: day of year (i.e., date of sampling event), flow state (i.e., whether
774 flowing or pooled), water temperature, topographic wetness index, contributing area, burn
775 frequency, elevation, and slope. We then extracted the conditional permutation importance for
776 each predictor variable (Strobl et al., 2008), which accounts for collinearity among other
777 predictors. A higher conditional variable importance indicates that the predictor variable has a
778 greater influence on model predictors for the out-of-bag samples used in model training. Lastly,
779 we calculated the root mean squared error (RMSE) between the predicted $\delta^{18}\text{O}$ and the
780 observed $\delta^{18}\text{O}$ to assess model performance. We found that day of year, flow state, and water
781 temperature were the most influential predictor variables (Figure S6). This further supports our
782 findings that evaporation and a decrease in surface water connectivity are the primary factors
783 influencing stream $\delta^{18}\text{O}$ compositions (see Figure 5 in the main text).

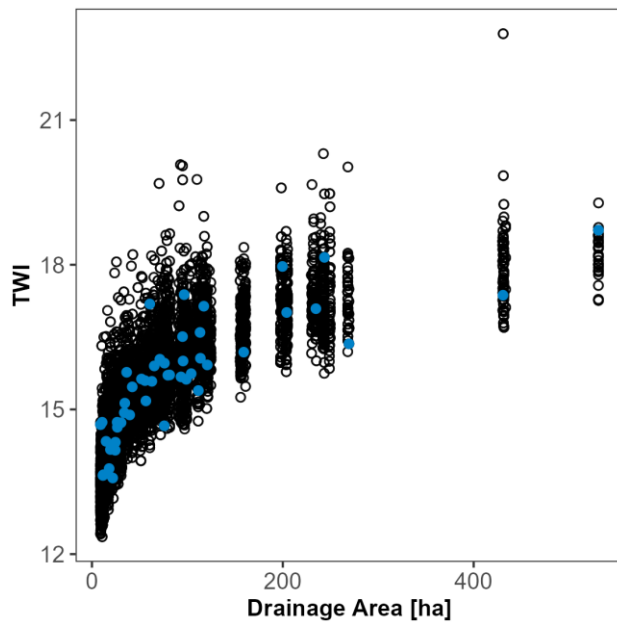
784

785

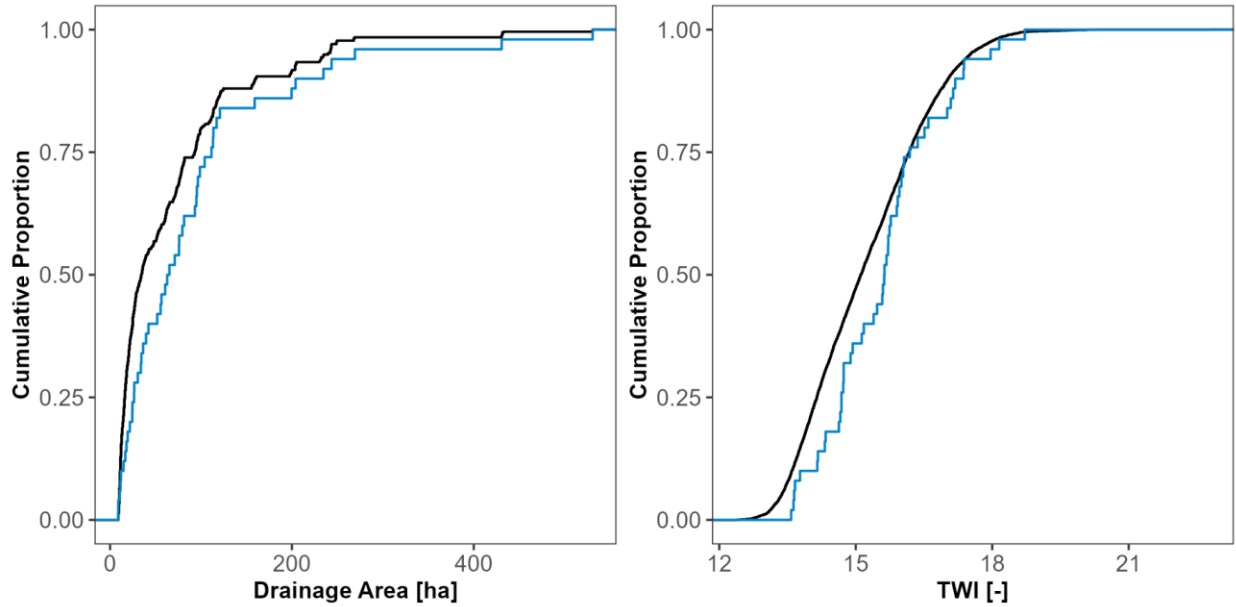
786 **Figures**



787
788 **Figure S1.** Distribution of drainage area and TWI for all stream network points at the site. The
789 red vertical lines indicate the 10 drainage area groups used to randomly distribute points, and
790 each bin was divided into 5 quantiles based on the TWI distribution.
791

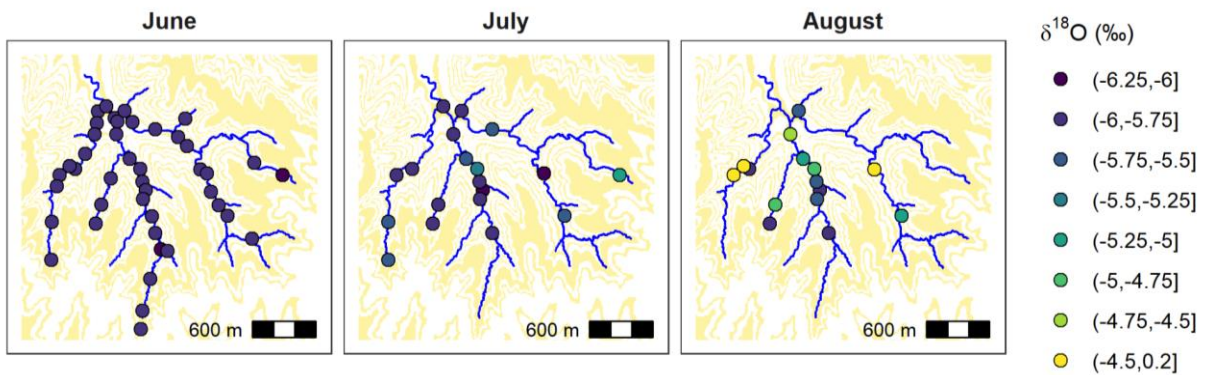


792
793 **Figure S2.** Distribution of drainage area and TWI for sampling sites (blue) and all stream
794 network points (black) at the site.
795



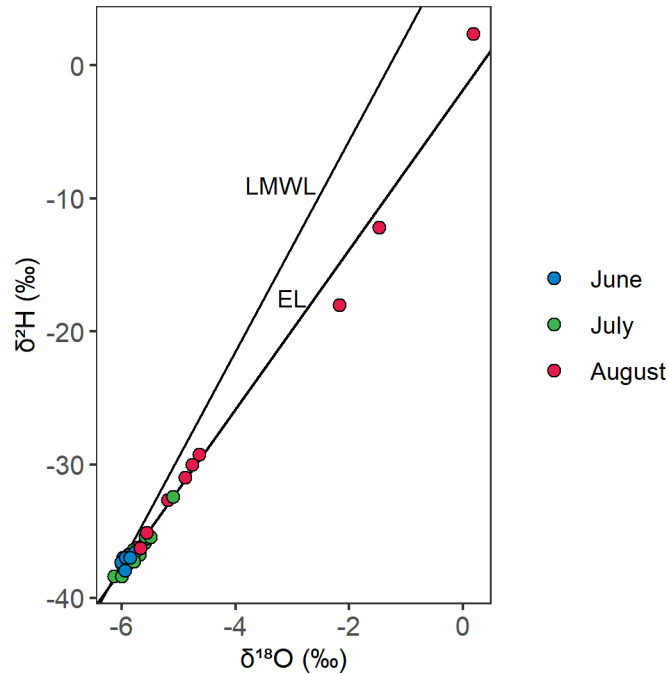
796
797
798
799
800

Figure S3. Empirical cumulative distribution functions (ECDFs) of drainage area and TWI for all stream points (black) and sampling sites (blue) for the site.

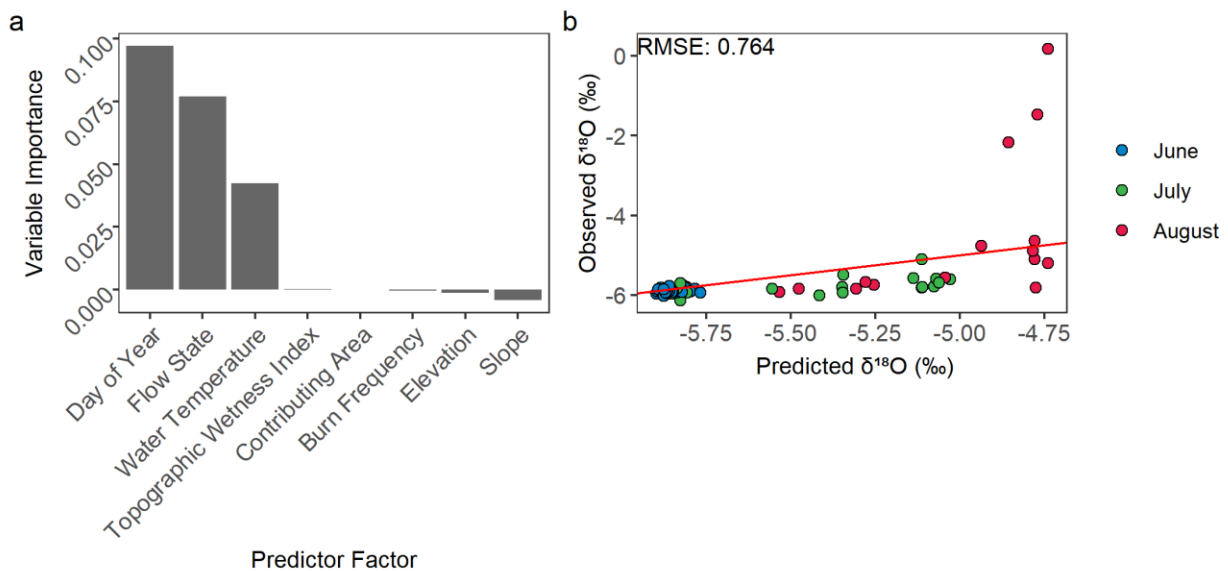


801
802
803
804
805
806
807

Figure S4. Spatial variation in $\delta^{18}\text{O}$ during the summer dry-down period. The estimated elevations at which limestone units outcrop the watershed are shown as yellow bands. These elevations are based on the average member thickness in the drilling log records at the Konza Prairie.



808
 809 **Figure S5.** Stream $\delta^{18}\text{O}$ and $\delta^2\text{H}$ in the South Fork of Kings Creek. Shown are the local meteoric
 810 water line (LMWL) and the evaporation line (EL). The LMWL ($\delta^2\text{H} = 7.93 \times \delta^{18}\text{O} + 10.28$, $R^2 =$
 811 0.97) is based on a long-term record of precipitation isotopes collected at Konza Prairie by the
 812 National Ecological Observatory Network (NEON, 2022).
 813



814
 815 **Figure S6.** Random forest model to predict $\delta^{18}\text{O}$ in the South Fork of Kings Creek. Shown are (a)
 816 predictor factors ordered according to decreasing conditional permutation importance and (b)
 817 model fit. The red line shows a 1:1 match between predicted and observed.
 818

819
820
821
822
823
824
825
826
827
828
829
830
831
832
833
834
835
836
837
838
839
840
841
842
843
844

References

- Addor, N., Nearing, G., Prieto, C., Newman, A. J., Le Vine, N., & Clark, M. P. (2018). A Ranking of Hydrological Signatures Based on Their Predictability in Space. *Water Resources Research*, 54(11), 8792–8812. <https://doi.org/10.1029/2018WR022606>
- Eng, K., Grantham, T. E., Carlisle, D. M., & Wolock, D. M. (2017). Predictability and selection of hydrologic metrics in riverine ecohydrology. *Freshwater Science*, 36(4), 915–926. <https://doi.org/10.1086/694912>
- Hothorn, T., Bühlmann, P., Dudoit, S., Molinaro, A., & Van Der Laan, M. J. (2006). Survival ensembles. *Biostatistics*, 7(3), 355–373. <https://doi.org/10.1093/biostatistics/kxj011>
- Lutz, S. R., Krieg, R., Müller, C., Zink, M., Knöller, K., Samaniego, L., & Merz, R. (2018). Spatial Patterns of Water Age: Using Young Water Fractions to Improve the Characterization of Transit Times in Contrasting Catchments. *Water Resources Research*, 54(7), 4767–4784. <https://doi.org/10.1029/2017WR022216>
- Miller, M. P., Carlisle, D. M., Wolock, D. M., & Wiczorek, M. (2018). A Database of Natural Monthly Streamflow Estimates from 1950 to 2015 for the Conterminous United States. *JAWRA Journal of the American Water Resources Association*, 54(6), 1258–1269. <https://doi.org/10.1111/1752-1688.12685>
- Strobl, C., Boulesteix, A.-L., Zeileis, A., & Hothorn, T. (2007). Bias in random forest variable importance measures: Illustrations, sources and a solution. *BMC Bioinformatics*, 8(1), 25. <https://doi.org/10.1186/1471-2105-8-25>
- Strobl, C., Boulesteix, A.-L., Kneib, T., Augustin, T., & Zeileis, A. (2008). Conditional variable importance for random forests. *BMC Bioinformatics*, 9(1), 307. <https://doi.org/10.1186/1471-2105-9-307>
- Warix, S. R., Godsey, S. E., Lohse, K. A., & Hale, R. L. (2021). Influence of groundwater and topography on stream drying in semi-arid headwater streams. *Hydrological Processes*, 35(5), e14185. <https://doi.org/10.1002/hyp.14185>